Determination of contrast-detail curves of mammography systems by automated image analysis [1]

N. Karssemeijer and M.A.O. Thijssen

University Hospital Nijmegen, Department of Radiology, PO Box 9101, Nijmegen, 6500 HB, The Netherlands

1. INTRODUCTION

Many phantoms have been designed to study mammographic image quality. Not all of these are suitable for use with digital systems. Especially, measurement of spatial resolution with line patterns does not seem appropriate, because microcalcifications, the smallest objects visible in mammograms, are better represented by dot patterns. A phantom in which dot patterns are applied is the CDMAM phantom that was developed at our institute (Figure 1). This phantom consist of a matrix of square cells with dots of varying size and contrast. In each of the 205 cells of the matrix one dot is at the center and another is positioned in a randomly selected corner. The observer's task is detection of the dots. Responses can be evaluated as percentages of correct detections per image. When using multiple readouts of phantom recordings the fraction of correct decisions can be determined per cell, i.e. as a function of object size and contrast. These fractions can be used to determine a contrast detail curve relating object size and contrast at some fixed detection threshold.

Measurement of contrast detail curves by human readout of multiple phantom images is tedious and time consuming. Therefore, we have developed a computer program which performs an automatic readout of the phantom recordings. The use of this program allows making quick and reliable comparisons of digital mammographic imaging procedures.

2. METHODS

In its simplest form fully automatic readout of digital phantom images is performed in three steps: (1) determination of position, orientation and scale of the phantom in the image matrix, (2) construction of templates of the dot objects in each of the four corners of each cell, and (3) selection of the cell corners in which the dots are most likely to be located using the ideal observer model. Computation of contrast detail curves can be performed by applying the program to a number of phantom images, and calculating the probability of detection for each cell. A more efficient procedure for determining these probabilities has also been implemented, making use of the central dot in each cell and estimation of background fluctuation.

2.1 Determination of grid position

For automated analysis of digital CDMAM phantom images, the exact position of each

[1] In: Digital Mammography, Ed: K Doi, M L Giger, R M Nishikawa, R A Scmidt, Elsevier (Amsterdam) pp 155-160, 1996

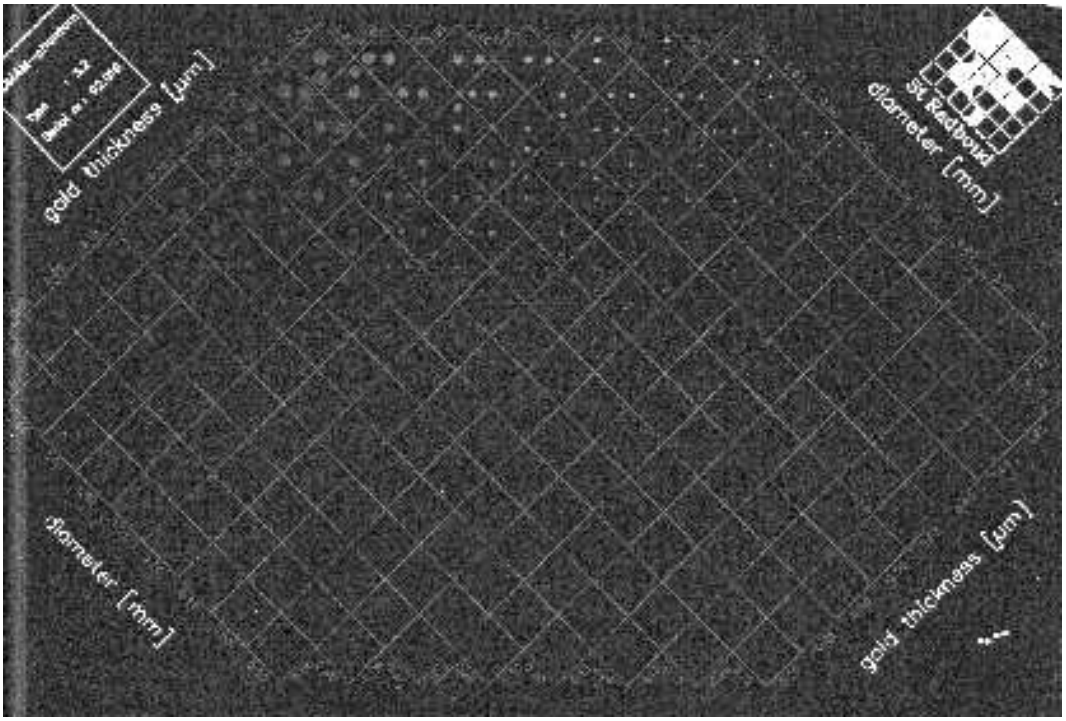

Figure 1: A digitally recorded X-ray image of the CDMAM phantom.

cell of the phantom must be known. In our approach the four corner points of each cell are determined, i.e. the centers of the grid line crossings. It is assumed that the phantom is positioned as such that grid lines in the direction of increasing contrast are at an angle in the interval [0,90).

Parts in the image matrix that are outside the phantom may contain unexposed bright areas that need to be removed before processing. Therefore, within a fixed region of interest at the center of the image matrix the mean pixel value and its standard deviation are calculated. All pixels outside a range of values around the mean are set to zero. After segmentation of the phantom, a trend correction is performed to remove low frequency components due sources like the Heel effect and light source inhomogeneity during digitization. For this purpose, in a moving window of 4mm $\times$ 4mm the median pixel value M_i is computed. Correction is performed by multiplying the image pixel-wise by I_{bg}/M_i, with I_{bg} the constant background pixel value after correction. By using the median, the influence of the grid line and dot pattern itself on the correction is minimal.

To determine the global position, scale and orientation of the phantom, a Hough transform is performed on the image at a reduced resolution of 400 micron per pixel. For all pixels within the segmented phantom area the gradient magnitude and orientation are calculated using a 3×3 Sobel operator. From the histogram of gradient magnitude values a threshold is determined which maps 20% of the pixels with highest magnitude. These pixels, which mainly are located at the grid pattern and at the borders of the brighter dots, are transformed to Hough space. This space can be viewed as an accumulator array

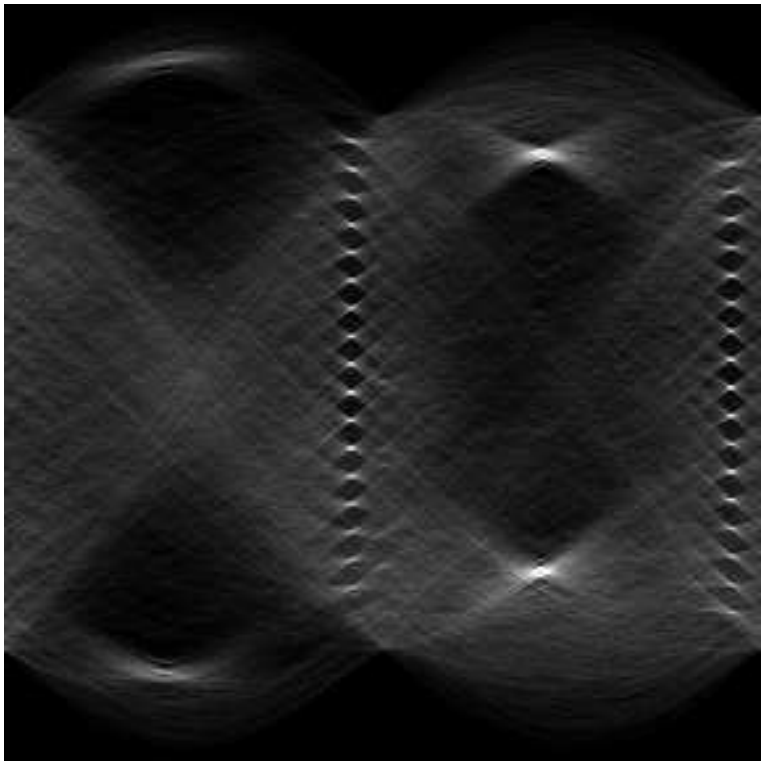

Figure 2: Hough transform of a phantom image in which grid lines are represented as two columns of peaks.

of parameter values representing all possible straight lines. For each selected pixel in the image the elements in the accumulator array representing straight lines through this pixel are incremented. In our implementation we we used the (ρ, θ) line parameterization:

$$\rho = x\cos(\theta) + y\sin(\theta). \tag{1}$$

Figure 2 shows the pattern obtained in Hough space. Each sinusoidal curve reflects the contribution of one pixel. Each peak at a crossing of many of such curves represents a straight line in the image. The regular grid line pattern of the phantom can be easily identified by the two columns of 17 peaks each, separated by an angle of $\frac{1}{2}\pi$.

To determine the orientation of the phantom in the image matrix the fluctuation $f(\theta)$ of values $h(\theta, \rho)$ in Hough space is determined by computing

$$f(\theta) = \sum_{\rho=\delta\rho}^{\rho_{max}} abs(h(\theta, \rho) - h(\theta, \rho - \delta\rho)), \tag{2}$$

and the orientation α of the grid lines is estimated by

$$\hat{\alpha} = \max_{\theta} \left[f(\theta) + f(\theta + \pi/2) \right]. \tag{3}$$

The distance between the grid lines D can be determined from the distance between the peaks in Hough space. To estimate this distance accurately the autocorrelation of the accumulator array columns at α and $\alpha + \frac{1}{2}\pi$ is calculated by

$$a(r) = \sum_{\rho=0}^{\rho_{max}-r} h(\alpha, \rho)h(\alpha, \rho + r) + h(\alpha + \pi/2, \rho)h(\alpha + \pi/2, \rho + r) \tag{4}$$

The maximum of $a(r)$ provides the estimate of the size D of the phantom cells. Given orientation α and scale D, only the exact position of the phantom in the image matrix needs to be resolved. For this purpose an array with 17 distinct peaks spaced at distances D is constructed and used as a template on the columns at α and $\alpha + \frac{1}{2}\pi$ of the accumulator array. The positions at which the template fits best determines the location of the phantom in image space.

With the estimated grid parameters the location of the grid line crossings can be computed. It turned out that these match closely to the image data, but not accurate enough. Small deviations occur due to geometrical distortion during the imaging procedure and due to the low Hough space resolution. Clearly, such deviations are not acceptable as they are larger than the smallest dots to be detected. Therefore, an additional matching procedure is implemented to optimize the position of each grid line crossing individually. In this procedure a template of a grid line crossing at the estimated orientation α is correlated with the image data within a small area (15×15 pixels) around the predicted crossing. The optimal location is determined as the one with the highest cross-correlation. At the boundary of the phantom this may sometimes fail, because no special templates at line-crossings at the boundary are used. Instead, a check on consistency of the final result is performed. If an outlying point is found this point is corrected by interpolation from the surrounding points.

2.2 Computation of contrast-detail curves

For each row of the phantom with dot diameter d the known coordinates of the cell corners allow construction of disc templates in each cell corner. This allows the use of the ideal observer model to detect the dots. The average pixel value under each template is calculated and the corner in which the average has the highest value is chosen. No noise-prewhitening is used. If the program is applied to a number of recordings the likelihood of correct detection can be computed for each cell. A more accurate procedure to estimate these probabilities was developed by using the contrast of the central dots in the cells as well, and by estimation of the background fluctuation for each object diameter from image data at the known non-signal locations.

From the detection probabilities measured in each cell, a contrast detail curve can be estimated for a given detection threshold. We use a model based interpolation scheme to

fit a curve through the data. In this model the probability of detection $p(d)$ of a dot of size d as a function of its contrast c can be described by a psychometric curve of the form

$$p(d) = \frac{0.75}{1 + e^{-f(C-C_T)}} + .25 \tag{5}$$

with C the logarithm of signal contrast $C = log(1 - e^{-\mu d})$. For the linear attenuation coefficient of gold we took $\mu = 190mm^{-1}$, and f is a free parameter to be fitted. Using the logarithm of contrast, the psychometric functions for most stimuli appear to have similar shapes [1]. Therefore, we could use a fixed value of f for all diameters. For fitting the curves through to the data we applied a least squares procedure for each diameter independently. A threshold at 62.5% correct responses is used for computing contrast detail curves, which is exactly halfway the psychometric curve. The dot and contrast sizes of the phantom have been corrected for a small bias caused by manufacturing.

3. RESULTS

The method has been applied to compare the quality of images recorded with a Siemens DIGISCAN 2C using HRV storage phosphor plates with digitized conventional images recorded with a mammographic film/screen system (Kodak MIN-RH/MIN-R). Digitization was performed with an Eikonix 1412 digitizer, using 0.1 mm 12 bits pixels. In a previous study it was shown that digitization using this setup did not notably reduce human reader performance [2]. Phantom images were recorded at an exposure level of 63 mAs, where the phantom was placed within 4 cm perspex. The average optical density of the exposed films was 1.3 OD. Figure 3 shows contrast details curves for both systems, obtained from automated readout of 8 exposures. The 8 film/screen images were also read by an experienced human reader, whose performance is represented in the upper curve in Figure 3. Results of the two automatic readout procedures that were developed can be compared in Figure 4, showing curves obtained from DIGISCAN exposures at 100 mAs.

4. CONCLUSIONS

It was found that the detection performance of the automatic readout system is significantly better than that of human observers. Automatic detection can be used, however, to reliably predict average human performance. It was also found that in the range of objects covered by the phantom the detection rate using the storage phosphor recordings is as good as when using digitized conventional mammography, where the comparison is made at an exposure level where the film/screen DQE is about at optimum. In general, all the larger dots were detected by the system, disallowing computation of contrast detail thresholds for dots larger than 1 mm. In Figure 4 it can be seen that the readout procedure using the central dots as well gives similar results, but is somewhat more precise.

Automatic readout of the CDMAM phantom provides a reliable and less time consuming alternative to human readout. Currently, it is tried to implement this method in the quality control protocol of the Dutch screening program. Such digital quality control systems may become very valuable when digital mammography is introduced in screening.

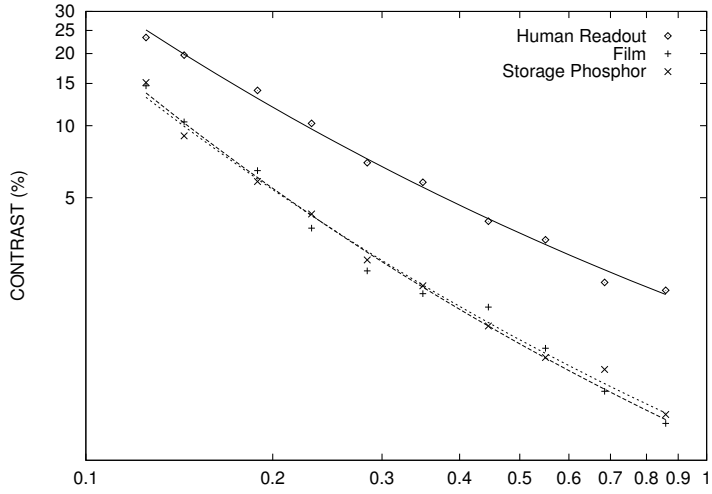

Figure 3: Contrast-detail curves showing the average performance of a human reader on conventional film ($\diamond$), the results of the automatic system on the same set of films after digitization (+), and on storage phosphor images recorded under the same conditions (x).

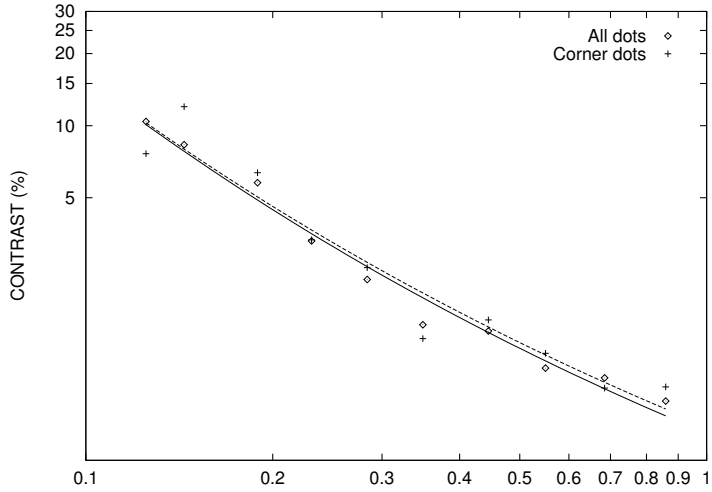

Figure 4: Contrast-detail curves showing results of the two procedures for automatic readout that were implemented.

REFERENCES

1. L.A. Olzak, J.P. Thomas, Seeing Spatial Patterns, in "Handbook of Perception and Human Performance" (Ed. K.R. Boff, L. Kaufman, J.P Thomas), Wiley,1987.
2. N. Karssemeijer, J.T.M. Frieling, J.H.C.L. Hendriks, Spatial Resolution in Digital Mammography, Investigative Radiology 28, 413-419 (1993)